AGU PUBLICATIONS

JGR

Journal of Geophysical Research: Space Physics

RESEARCH ARTICLE
10.1002/2017JA024300

Key Points:
- Solid propellant rocket destruction in the ionosphere on 9 December 2009
- VHF meteor radar detected electron density irregularities caused by dust of the rocket remains in the mesosphere
- Dust-associated mesospheric irregularities with a temporal scale of 0.1 s and a spatial scale of a few to tens of meters

Correspondence to:
A. Kozlovsky,
alexander.kozlovsky@oulu.fi

Citation:
Kozlovsky, A., S. Shalimov, and M. Lester (2017), Mesospheric plasma irregularities caused by the missile destruction on 9 December 2009, *J. Geophys. Res. Space Physics*, *122*, 6696–6707, doi:10.1002/2017JA024300.

Received 25 APR 2017
Accepted 30 MAY 2017
Accepted article online 31 MAY 2017
Published online 13 JUN 2017

Mesospheric plasma irregularities caused by the missile destruction on 9 December 2009

Alexander Kozlovsky[1], Sergey Shalimov[2,3,4], and Mark Lester[5]

[1]Sodankylä Geophysical Observatory, Sodankylä, Finland, [2]Institute of Physics of the Earth RAS, Moscow, Russia, [3]Space Research Institute, Moscow, Russia, [4]National Research Center "Kurchatov Institute", Moscow, Russia, [5]Department of Physics and Astronomy, University of Leicester, Leicester, UK

Abstract On 9 December 2009 at about 07 UT a solid propellant 36.8 t ballistic rocket was self-destroyed at an altitude of 170–260 km, at a distance of about 500 km to the east of Sodankylä Geophysical Observatory (SGO, 67°22′N, 26°38′E, Finland). After 2–3 h the SGO meteor radar (operating at a frequency 36.9 MHz) received unusual echoes, which indicate turbulence of ionospheric plasma (irregularities of electron density) with a temporal scale on the order of 0.1 s and a spatial scale of a few to tens of meters. The turbulence occurred at a height of about 80 km and was localized in several areas of about 60 km in horizontal scale. Line-of-sight velocity of the irregularities was up to a few tens of meters per second toward the radar. The event occurred in the winter high-latitude mesosphere during extremely low solar and geomagnetic activity. Aerosol particles caused by the missile explosion played a key role in producing the electron density irregularities. As a possible explanation, we suggest that sedimented by gravity and, hence, moving with respect to the air, charged aerosol particles (presumably composed of aluminum oxide) might produce meter-scale irregularities (electrostatic waves) via dissipative instability, which is a mechanism analogous to that of the resistive beam-plasma instability.

1. Introduction

The Russian military missile "Bulava" is a submarine-launched three-stage solid propellant 36.8 t ballistic rocket. On 9 December 2009 at about 07 UT a test launch of such a missile was performed from the White Sea (see a map in Figure 1). Because of a technical problem, the missile was self-destroyed soon after the launch at a height of about 200 km. Illuminated by the Sun, the combustion products of the fragments of the rocket formed a luminous spiral in the dawn sky [see, e.g., *Chernouss et al.*, 2012, Figure 4], so that inhabitants of Northern Norway and Sweden observed a spectacular phenomenon, which was later reported in newspapers as the "Tromso (or Norway) spiral." Using photos taken in different places in Northern Norway, *Spell* [2009] has calculated that the event occurred over the Kola Peninsula (Russia) within the area indicated by the green circle in the map in Figure 1, and the center of the event was located at about 170–260 km altitude.

Products of the explosion, presumably including long-lived metallic ions like aluminum or/and aluminum oxides ionized by the sunlight, were spread into a large area at altitudes which include the lower ionosphere (80–140 km heights). After 2–3 h they continued their rapid spreading and reached the region of Sodankylä Geophysical Observatory (SGO, 67°22′N, 26°38′E, Finland) about 500 km westward of the explosion point. Between 0900 UT and 1030 UT the SGO ionosonde observed near the zenith a sporadic *E* layer believed to be composed of the ionized remains.

The ionosonde observations were presented in *Kozlovsky et al.* [2014], where the focus was on the processes of transport (spreading) of the remains of the missile in the ionosphere. Also, *Kozlovsky et al.* [2014] reported that at the same time the meteor radar (MR) at SGO detected unusual clustered targets (color dots in Figure 1), which were attributed to reflections from the remains. It was briefly mentioned that these MR detections might be similar to that of the polar mesosphere summer echoes (PMSE), but a detailed investigation of the MR reflections was out the scope of that paper. Nevertheless, the nature of these MR signals appeared to be a challenging problem deserving a separate study.

The present paper is an attempt to investigate a specific reflection of the meteor radar signals from the irregularities caused by the scattered remains of the exploded missile. First, we briefly describe the principles of the MR operation and point out unusual features of the detections during the event. Second, we

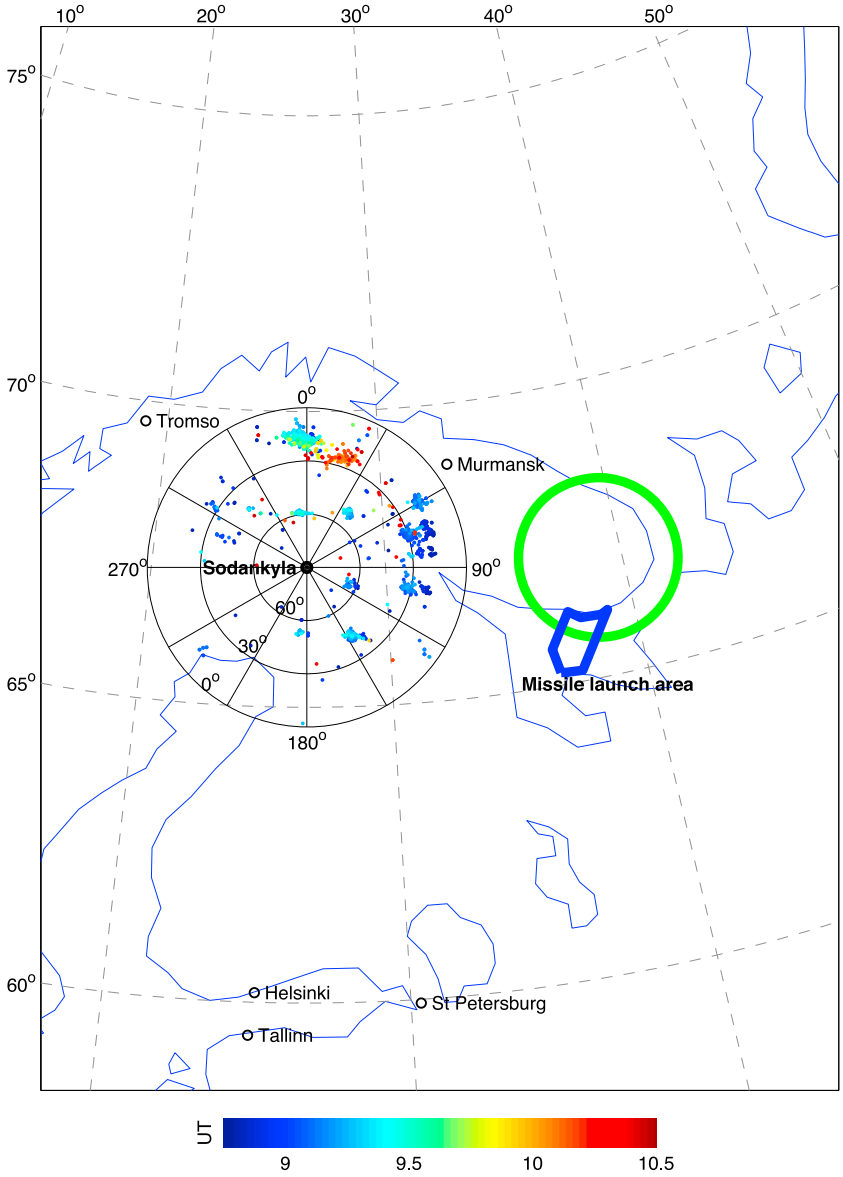

Figure 1. Map of the region. The closed blue line outlines the missile launch area in the White Sea. Green circle shows position of the sky spiral over Kola Peninsula. Colored dots around Sodankylä indicate the targets detected by the meteor radar between 0830 UT and 1030 UT. The colors of the dots (from dark blue to brown) correspond to the time of detection. The polar diagram centered at Sodankylä indicates azimuth and zenith angles of the targets.

investigate the MR data to specify the characteristics of the plasma irregularities which were responsible for the observed detections. Third, we summarize the experimental data on the irregularities and the background conditions. Finally, we suggest a possible physical mechanism for the plasma irregularities and present numerical estimations to support the validity of this mechanism.

2. Meteor Radar Observations

Meteor radars are designed to locate the ionizing trails of meteors in the mesosphere at heights between 70 and 110 km [*Hocking et al.*, 2001]. The SGO MR is an all-sky interferometric meteor radar (SKiYMET), which transmits short bursts (pulses) of very high frequency (36.9 MHz) radio waves. The transmit antenna has a broad radiation pattern designed to illuminate a large expanse of the sky.

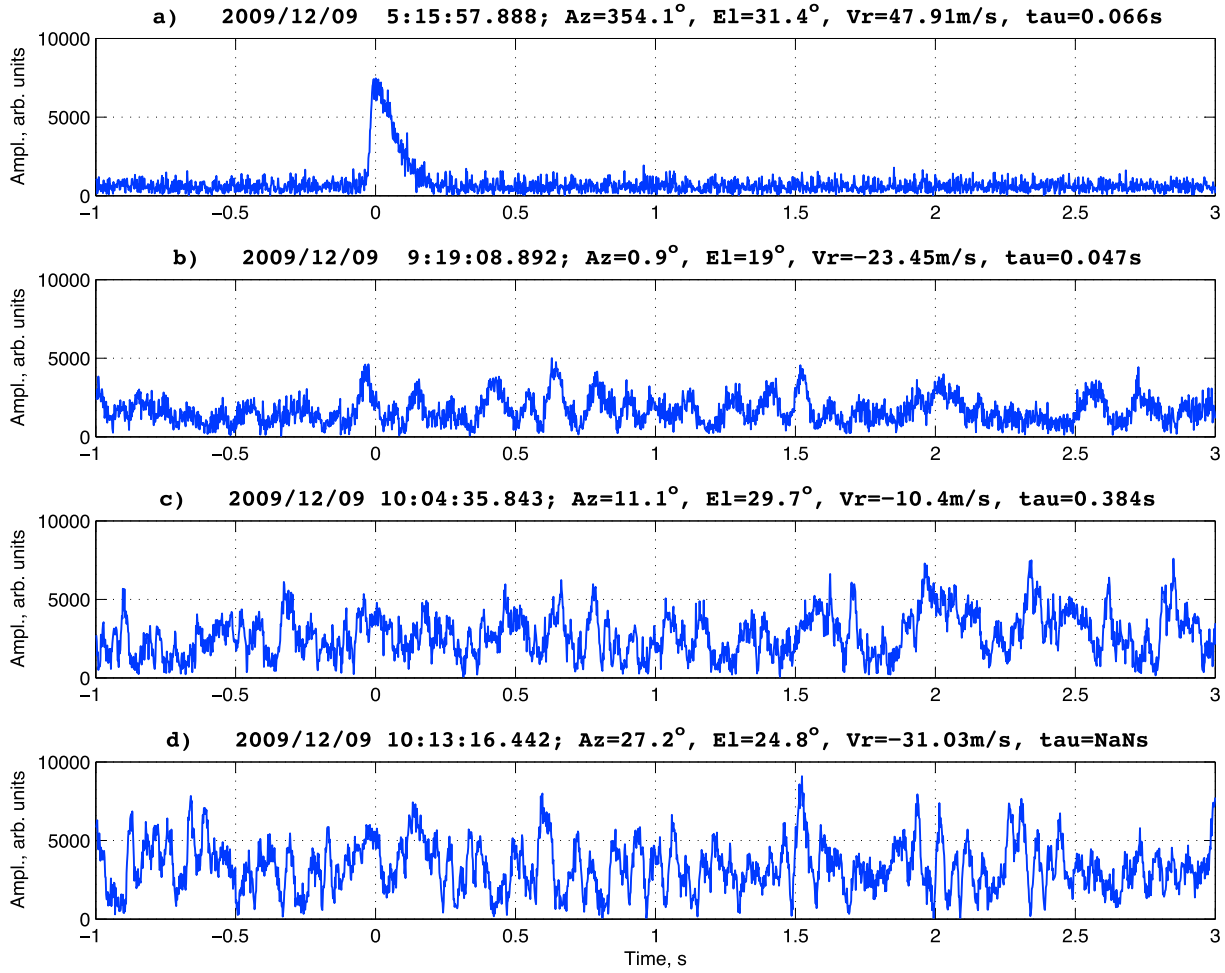

Figure 2. (a) Amplitude of received signals corresponding to a meteor detection and (b–d) echoes from the irregularities associated with remains of the missile. Zero time corresponds to the time of meteor detection.

The characteristic features used to distinguish meteor echoes from other signals include their rapid onset, relatively short duration (typically less than 2 s), and quasi-exponential decay [*Hocking et al.*, 2001]. Processing software on the MR analyzes the received signals and selects only those signals which based on the above characteristics are believed to be from meteor trails. For those detections selected as meteors, short 4 s records of the amplitude and phase of the received signals are archived. A typical example of such a record is shown in Figure 2a, where the amplitude of the signals received at one of the five MR antennas is presented versus time. Zero time approximately corresponds to the time of meteor detection.

The receiving system determines the azimuth, elevation, range, and Doppler velocity of the targets. The range may be determined with a 70 km ambiguity because of the 2144 kHz interpulse frequency of MR transmissions. To reduce the range ambiguity, the MR data analysis algorithm assumes that meteor trails are at heights between 70 and 110 km, such that meteor trails detected at high enough elevation may be located unambiguously.

For each detection identified as a meteor echo the decay time, i.e., namely, the half-life time, $\tau_{1/2}$, for which amplitude of the received signal decreases by half, is calculated from the width of the autocorrelation function of the received signal. However, in some cases the autocorrelation function is too broad, so that the standard procedure is not able to determine the decay time and a missing value is given for the decay time. Such echoes, referred to as nonexponentially decayed (NED), are detected during intense meteor showers and sometimes during substorms [*Kozlovsky and Lester*, 2015]. In the latter case the NED echoes are not associated with meteors. Many NED echoes were detected after the missile explosion.

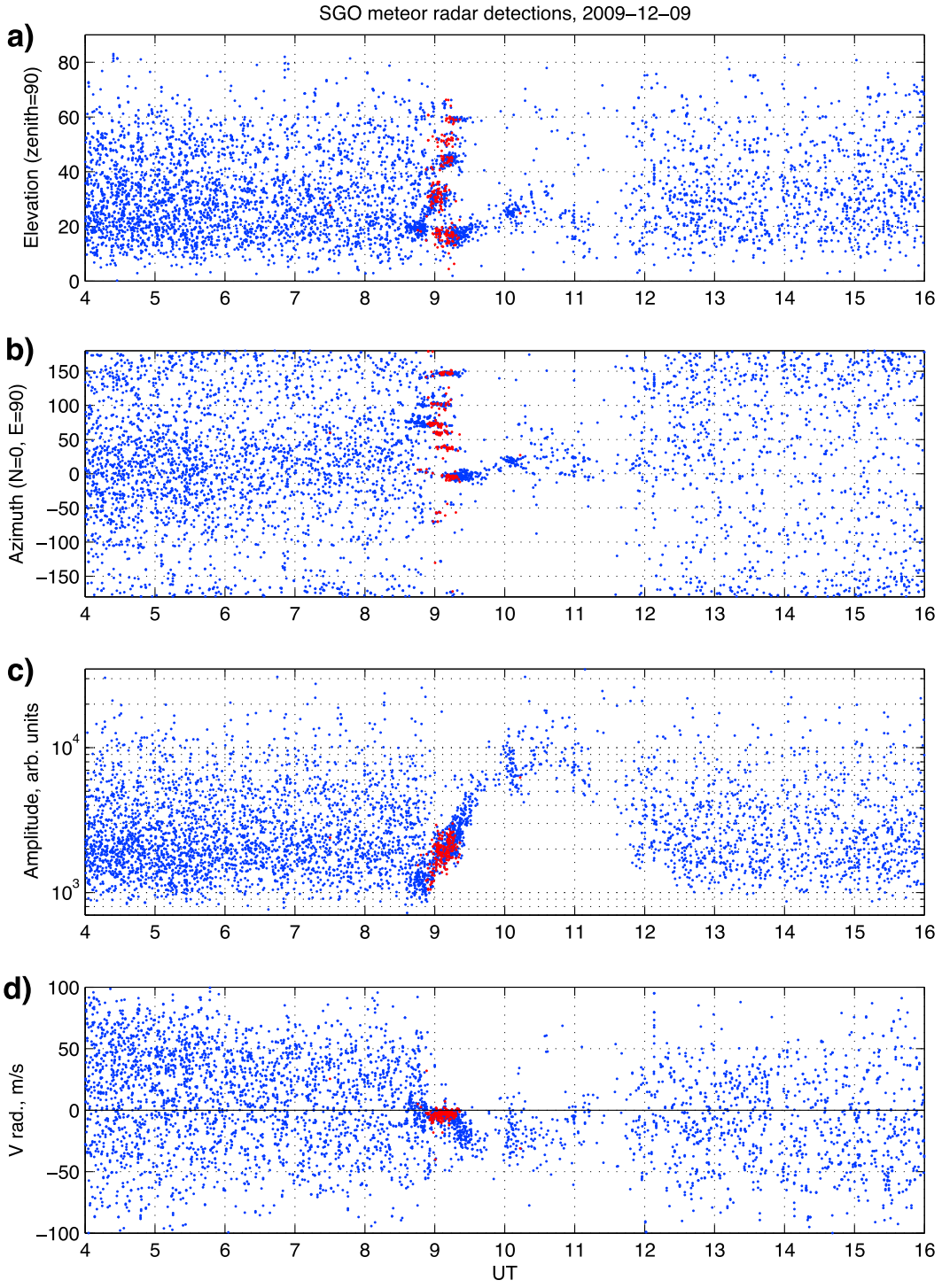

Figure 3. An overview plot showing parameters of the MR detections during 04–16 UT on 9 December 2009. The parameters are (a) elevation, (b) azimuth, (c) amplitude of received signal, and (d) Doppler line-of-sight velocity. Red dots indicate NED echoes for which decay time was not determined.

Figure 3 is an overview plot showing parameters of the MR detections between 04 and 16 UT on 9 December 2009. The parameters are elevation, azimuth, amplitude of received signal, and Doppler line-of-sight velocity. Red dots indicate NED echoes. Before 0840 UT the radar normally detected meteor trails, which was characterized by typical distributions of all parameters. The first indication of the missile

remains appeared at 0840 UT in the form of a cluster of targets at elevation 20° and azimuth 75°. Between 0900 and 1030 UT the MR detected predominantly clustered targets related to the remains, compared to which the number of meteors was negligible. From 1030 to 1200 UT very few detections were recorded because of an enhanced noise level due to reflections from the dense sporadic *E* layer [*Kozlovsky et al.*, 2014].

Colored dots in Figure 1 show the azimuth and elevation directions from the MR toward targets between 0845 and 1030 UT, when the great majority of the targets were those related to the remains. The color of the dots indicates time of the detection, accordingly to the color bar in the bottom.

Examples of the amplitude variations for some clustered detections are shown in Figures 2b–2d, where quasiperiodic modulation with an irregular periodicity on the order of 0.1 s is seen. The shape of the modulation is clearly different from that of meteor trails, although individual peaks of the oscillations might be identified as meteors. For some of these signals the decay time was determined (e.g., Figures 2b and 2c), whereas some of them were identified as NED (e.g., Figure 2d).

In fact, the observations in Figures 2b–2d indicate an unusual localized turbulence of the ionospheric plasma with a temporal scale on the order of 0.1 s. Given that the radar wavelength is 8.13 m, the spatial scale of the irregularities would be on the order of 4 m in the case of Bragg scattering or tens of meters in the case of the incoherent scattering or Fresnel reflection. Irregularities in the electron density associated with the turbulence could be responsible for the unusual detections by the meteor radar. The main purpose of the present paper is to investigate further the origin of such turbulence.

3. Characteristics of the Plasma Irregularities

3.1. Height of the Reflections

Due to the 2144 kHz interpulse frequency of the MR transmissions, distances to the targets are measured with the 70 km range ambiguity. An unambiguous location of meteors is possible because it is known that most of meteor trails occur at certain heights (typically between 80 and 100 km). In our case, we do not know a priori a height range for the nonmeteor targets, although with some reasonable assumptions the height estimation appears to be possible.

The polar diagram in Figure 1 shows the directions (azimuth and elevation) of the targets indicated by colored dots, where the color of the dots corresponds to the time of detections. This plot shows that the targets formed localized clusters, each of which was observed for about 20–30 min. For instance, at about 0900 UT there were a few clusters in the east of Sodankylä, at about 0930 UT a cluster was observed in the north, and at about 1000 UT a cluster (red dots) appeared just east of north.

We may assume that the heights of all targets within a cluster do not differ significantly. After that, we selected one specific cluster that detected during 0945–1030 UT in the azimuth range of 8°–30° at elevation of 15°–35° and considered it in more detail. These detections were of the largest amplitude and, hence, the best signal-to-noise ratio, and they correspond to the cluster at about 1000 UT in Figure 1 (red dots). In total, 70 detections of this cluster were selected.Then, for every detection we calculated the possible positions of the target (i.e., height and distance along Earth's surface) assuming various possible ranges *R* and taking into account the range ambiguity:

$$R = R_0 + 70 \ \text{km}\cdot n, \quad (n = 0, 1, 2, \ldots) \tag{1}$$

The positions of the targets are shown in Figure 4 as asterisks in the frame of the height and distance along the Earth's surface. The asterisks form clusters of points corresponding to various *n* (shown in Figure 4 are six of such clouds) and each cluster of asterisks group about a certain straight line, indicated as dashed red lines. The lines have different slopes decreasing from positive at closer ranges to negative at further ones. A nonzero slope, however, indicates that targets belonging to this cluster are at different heights, and moreover, the height tends to increase or decrease with the distance, which is not realistic. Hence, only the group where the line has zero slope, corresponding to the third group of asterisks in Figure 4, represents the most likely situation. This leads to the conclusion that the targets were located at about 80 km height. Correspondingly, the horizontal size of the cluster is on the order of 60 km.

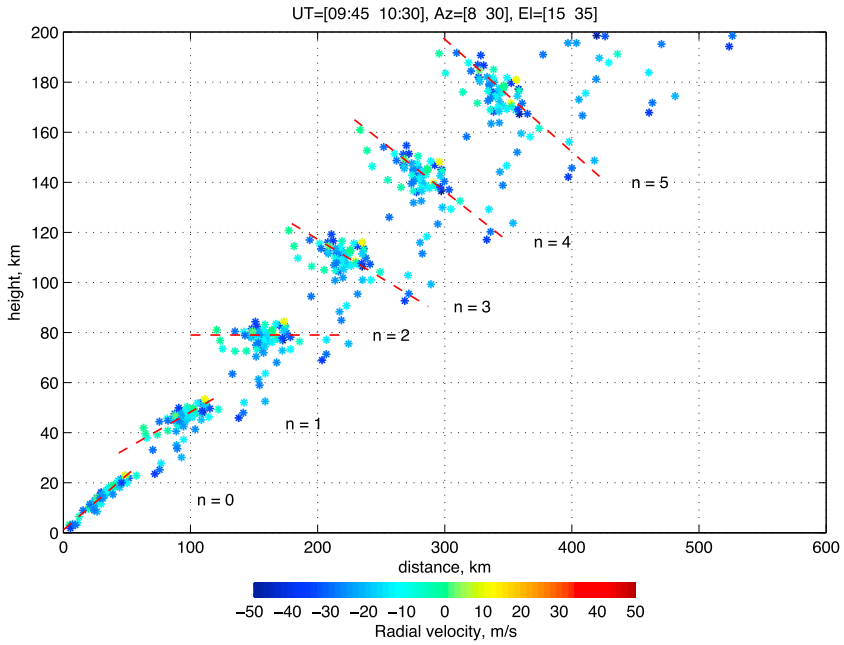

Figure 4. Possible positions of meteor radar targets as a function of the height and distance along the Earth's surface for different range assumptions within the 70 km range ambiguity. Color of the asterisks indicates the line-of-sight velocity accordingly to the color bar in the bottom.

3.2. Time Scale and Velocity of the Irregularities

As mentioned previously, the examples in Figures 2b–2d show an irregular quasiperiodic modulation of the amplitude of the detections with a period on the order of 0.1 s. We now consider the modulation of returns from the irregularities related to remains (referred below as IRRs) in more detail. The averaged amplitude spectrum of the modulation of MR returns during 0930–1030 UT is shown in Figure 5 (red curve), which

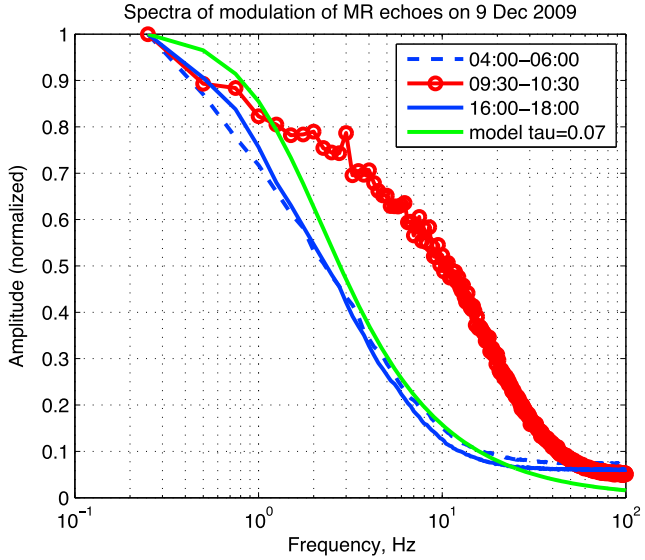

Figure 5. Averaged amplitude spectrum of the modulation of MR returns during 0930–1030 UT (red curve), which corresponds to the most intense reflections from the irregularities related to remains. Blue dashed and solid curves show averaged spectra for time intervals 0400–0600 UT and 1600–1800 UT, respectively, which correspond to detections of meteors before and after the event. The green curve shows a model amplitude spectrum for meteor detection.

corresponds to the most intense reflections from the IRRs. For comparison, the blue dashed and solid curves in this plot show averaged spectra for time intervals 0400–0600 UT and 1600–1800 UT, respectively, which correspond to detections of meteors before and well after the event.The green curve in Figure 5 show a model amplitude spectrum, $A_m(f)$, calculated as Fourier transform of an exponentially decaying signal, $\exp(-t \ln 2/\tau_{1/2})$, which corresponds to typical detection of an underdense meteor trail:

$$A_m(f) \propto \frac{1}{\sqrt{\left(\ln 2/\tau_{1/2}\right)^2 + (2\pi f)^2}} \quad (2)$$

We use here the half-life time, $\tau_{½}$, equal to 0.07 s, which is a typical decay time around 90 km heights where the majority of meteors are detected. These parameters were obtained from the MR observations during the day before the events (i.e., 8 December 2009).

Figure 5 shows that spectra before and after the event are similar to the model spectrum of meteors, whereas the spectrum corresponding to IRRs is essentially different. The IRR spectrum indicates frequencies from a few to about 10–20 Hz, i.e., a time scale on the order of 0.1 s, which was already mentioned above on the basis of visual inspection of individual detections.

Figure 3d presents the line-of-sight velocity of MR detections. The IRR detections show preferably negative (i.e., toward the radar) velocities up to a few tens of meters per second. We cannot derive vector velocity from these data, but they provide some velocity limits, which should be taken into account in the interpretation below. Notably, the velocity direction toward the radar agrees with (although, does not prove) downward motion of irregularities.

4. Main Results

To summarize, the above analysis indicates the clusters of returns come from an altitude of ~80 km and there is evidence of a periodicity of ~0.1 s at a spatial scale of a few to tens of meters. The velocity of the irregularities does not exceed a few tens of meters per second. Furthermore, it is worth mentioning the background conditions of the event. First, geomagnetic activity was extremely low at this time, namely, during 8–9 December *ap* index was zero and magnitudes of magnetic variations in SGO (including daily variations) did not exceed 10 nT [*Kozlovsky et al.*, 2014]. So that effects of the large-scale electric field can be neglected. Second, the event occurred at high latitudes where the magnetic field is nearly vertical. Third, the mesospheric temperature at this location in December does not change essentially from year to year [e.g., *Lukianova et al.*, 2015], and around 80 km heights it is typically about 220 K [*Shepherd et al.*, 2004; *Kaifler et al.*, 2017], which is relatively high. Fourth, dust or aerosol particles after the missile explosion are likely to play a key role in producing the electron density irregularities, since number of these particles would be expected to be unusually high.

Presented above summary of the experimental data on the irregularities and the background conditions is the main and the most important result of the study. In the following we discuss possible physical mechanisms for the plasma irregularities.

5. Interpretation and Discussion

Solar and geomagnetic activity was extremely low during the event, so that effects of the large-scale electric field may be neglected. Hence, the mechanisms requiring strong enough external electric field like, e.g., gradient drift instability, unlikely might be responsible for detected irregularities.

Obviously, dust or aerosol particles after the missile explosion are likely to play a key role in producing the electron density irregularities. Hence, one might assume that possible mechanism for such irregularities might be similar to that suggested by *Chau et al.* [2014] for nonspecular meteor trails from non-field-aligned irregularities. Such echoes were qualitatively explained by the presence of charged dust forming from the meteoric material immersed in a turbulent flow, which could lead to meter-scale turbulence. This scenario requires significant turbulence of neutral atmosphere. In particular, in the case presented in *Chau et al.* [2014] clear signature of flow shear was observed. However, as was shown above, in our case the line-of-sight velocity of irregularities does not indicate a flow shear. This is further illustrated in Figure 4, where the color of the asterisks shows the line-of-sight velocity accordingly to the color bar in the bottom. One can see that at all

heights the velocity is up to a few tens of meters per second toward the radar and dependence on the height (i.e., signature of a flow shear) is not seen.

Looking through literature, we found one suitable mechanism, which satisfies the conditions listed above and might explain generation of the irregularities. Earlier, *Trakhtengerts* [1994] proposed this mechanism to explain the polar mesospheric summer echo (PMSE). In the following we consider this mechanism, which does not require a hypothesis of atmospheric turbulence and is solely based on the presence of aerosols. Sedimented by gravity and, hence, moving with respect to the air, charged aerosol particles can produce meter-scale irregularities (electrostatic waves) via a dissipative instability, a mechanism which is analogous to that of the resistive beam-plasma instability. Below we estimate applicability of this mechanism taking into account the specific parameters corresponding to the IRR case.

5.1. Charged Aerosol Particles and Initial Conditions

5.1.1. Aerosol Particles

Typically, solid rocket propellants contain a metal (aluminum), an oxidizer (e.g., ammonium perchlorate, NH_4ClO_4), and a binder-like polyurethane [*Silant'yev*, 1964]. Indeed, optical observations of the event showed a distinctive turquoise color [*Platov et al.*, 2013], which indicated aluminum monoxide molecules (AlO). According to the chemistry of metallic ions [*Brasseur and Solomon*, 1984; *Plane*, 2002], these molecules and their products are ionized by sunlight and certain reactions occur to produce particulates of aluminum oxide (Al_2O_3). The aluminum oxide particulates are able to capture ionospheric electrons, so that negatively charged dust (or so-called dirty/dusty plasma) is created through the chemical reaction

$$Al_2O_3 + e^- \rightarrow Al_2O_3^- . \tag{3}$$

This is similar to the artificial dusty plasma production in the first Charged Aerosol Release Experiment when during the in-flight engine firing of solid rocket motors 111 kg of Al_2O_3 were released in the ionosphere at 280 km altitude [*Bernhardt et al.*, 2011]. The motor produced aluminum oxide particulates in the 100 nm to 10 μm size range with a peak in the size distribution at 1 μm [*Bernhardt et al.*, 2012]. In our case, products of the missile explosion were released at about 170–260 km altitude. Being involved in both horizontal transport and vertical sedimentation, after about 2–3 h they were detected at 80 km altitude in the vicinity of SGO. Initially, the particulates might be of different sizes, but here we assume that all aerosol particles are of the same size of 100 nm (in radius); that is, only the lightest particles of the distribution are expected to be left in the mesosphere after 2–3 h of sedimentation (additionally, this assumption is discussed in the end of section 5.2).

5.1.2. Sedimentation of Aerosol Particles

The aerosol particles are sedimented in the atmosphere due to gravity. The velocity of the sedimentation with respect to the air, V_0, is directed vertically and determined according to the balance of gravity and friction forces:

$$m_a g = m_a \nu_a V_0 \;\Rightarrow\; V_0 = g/\nu_a, \tag{4}$$

where g is gravity, m_a is the aerosol particle mass, and ν_a is the effective collision frequency of aerosol particles with neutrals which is given by

$$\nu_a = \frac{9\eta}{2\rho_a r_a (r_a + 2l)}, \tag{5}$$

where ρ_a is the aerosol mass density, η is the dynamic viscosity, r_a is the aerosol particle radius, and l is the collision free path of air molecules. Here and below we neglect flows of the neutral atmosphere (i.e., the velocity of the air is zero).

5.1.3. Charge of Particles

Charged components of the ambient air are electrons and positive ions, which have initial steady state velocities, V_{0e} and V_{0i}, equal to zero. The quasi-neutrality condition for charged components in the initial steady state is

$$en_{0i} = en_{0e} + Zen_{0a}, \tag{6}$$

where e is the elementary charge, n_{0i} and n_{0e} are density of ions and electrons, and n_{0a} and Z are density and charge (elementary charge units) of aerosol particles.

Electric charge of a dust particle is determined by the balance of electron and ion fluxes collected at the surface of the particle. Due to the higher mobility of the electrons, aerosol particles typically become negatively charged. In the dayside ionosphere photodetachment and photoionization may affect the value and even sign of the dust charge [*Klumov et al.*, 2005]. Indeed, rocket experiments in the daytime lower ionosphere have shown positively and negatively charged dust grains at altitudes below 78 km, although at higher altitudes only negatively charged grains were detected [*Robertson et al.*, 2014]. Therefore, in our consideration we can assume negatively charged aerosols at altitudes near 80 km. At this height for the particles of selected size (r_a), the Debye length (r_D), and the collision free path of ions (electrons) ($l_{i(e)}$) the following condition is satisfied:

$$r_a << r_D << l_{i(e)}. \tag{7}$$

Under these conditions, the orbit motion limited theory is applicable and the following equation is derived from the equality of the electron and ion fluxes recombining on the grain surface [*Fortov et al.*, 2006]:

$$\exp(-z) = \frac{n_{0i}}{n_{0e}} \left(\frac{\mu}{\tau}\right)^{1/2} (1 + z\tau), \tag{8}$$

where

$$z = \frac{|Z|e^2}{r_a T_e}, \quad \tau = \frac{T_e}{T_i}, \quad \mu = \frac{m_e}{m_i}.$$

Here $T_{i(e)}$ and $m_{i(e)}$ are the temperature and mass of ions (electrons).

Solving (8) for an isolated grain in a quasi-neutral plasma and typical lower ionospheric conditions ($\tau = 1$ and $m_i \approx 100 m_u$, where m_u is the atomic mass unit), we obtain $z \approx 4.2$. This gives for a grain of 100 nm radius in warm winter mesosphere ($T_i \approx T_e \approx 220$ K), a typical grain charge on the order of $Z \approx 5$–6 elementary charge units.

5.1.4. Density of Aerosol Particles

An important parameter is the ratio of the charge density of the dust component to that of electrons:

$$P = \frac{|Z| n_a}{n_e}, \tag{9}$$

As mentioned above, the unique IRR case most probably occurred due to an unusually high number density of dust particles (i.e., large P). However, if the density of the particles was too large ($P > 1$), the majority of the electrons would be attached to the particles, so that the density of free electrons would be low. In such a case formation of essential electron density irregularities and even any reflection of the radio wave is hardly possible.

Moreover, with a lack of free electrons, the charge of the dust particles would be decreased, which also prevents the instability. Indeed, for $P < 1$, the grain charge is close to the charge acquired by an isolated grain, whereas for $P > 1$ the grain charge decreases appreciably [*Fortov et al.*, 2006]. Correspondingly, for $P > 1$ the density of free electrons decreases.

Thus, the unusual radar reflections indicate unusually large P, but on the other hand if $P > 1$ any radar reflection would be hardly possible because of low electron density. Hence, further we assume that $P \leq 1$ (additionally, this assumption is discussed in the end of section 5.2).

5.2. Instability Grows Rate

In describing the instability *Trakhtengerts* [1994] used quasi-hydrodynamic equations for the charged components (ions, electrons, and aerosol particles) and Maxwell's equation for the electric field and the space charge. For small harmonic perturbations at frequency ω, the following dispersion equation was obtained in the linear approximation:

$$1-\frac{\omega_a^2}{\omega(\omega+iv_a)}+\frac{i4\pi\sigma_i}{\omega-kV_0+ik^2D_i}+\frac{i4\pi\sigma_e}{\omega-kV_0+ik^2D_e}=0, \tag{10}$$

where v_a is determined by (5), $\omega_a=\sqrt{4\pi n_{0a}Z^2e^2/m_a}$ is the aerosol plasma frequency, k is the wave number along the relative velocity V_0, and $D_{i(e)}=T_{i(e)}/m_{i(e)}v_{i(e)}$ and $\sigma_{i(e)}$ are the ion and electron diffusion coefficients and conductivities, respectively.

Below we analyze the dispersion equation (10) in the same way as *Trakhtengerts* [1994] made but for different conditions and parameters, as was considered above. Near the instability threshold and with taking into account $(\omega-kV_0)^2<<k^4D_e^2$ (which is correct for mesospheric conditions [*Trakhtengerts*, 1994]) the following dispersion relation was obtained from (10):

$$\omega=kV_0\left(1-\frac{1}{2d}\pm\frac{1}{2d}\sqrt{1-\frac{4v_aD_i}{V_0^2}d}\right), \tag{11}$$

where

$$d=1+\frac{v_a}{4\pi\sigma_i}\left(1+\frac{\delta}{k^2r_{Di}^2}\right).$$

Here r_{Di} is the ion Debye radius and $\delta=n_{0e}/n_{0i}$. The condition $\mathrm{Im}\omega=0$ demands the expression under radical to be positive. It leads to the necessary instability condition $4v_aD_id/V_0^2\le1$, from which, with taking into account (4), the instability criterion is obtained as

$$V_0\ge V_{\mathrm{thr}}\equiv[4(1+\delta)D_ig]^{1/3}. \tag{12}$$

Taking into account that for the conditions of interest $d\approx1$ and $4v_aD_id/V_0^2<1$, and using (10) and (11), one can simplify the equation for the instability threshold as

$$\left(\frac{\omega_a}{v_a}\right)^2_{\mathrm{thr}}\approx\left[1+\frac{1}{k^2r_{Di}^2}(1+\delta)\right], \tag{13}$$

The instability generates irregularities of the characteristic scale

$$\lambda_{\mathrm{opt}}\approx\frac{2\pi}{y_m}\frac{D_i}{V_0}, \tag{14}$$

where the dimensionless parameter γ_m depends on δ and may vary between 0.1 and 1 near the minimum of the instability threshold [*Trakhtengerts*, 1994]. The instability growth rate near the threshold is determined by the expression

$$\gamma_m\approx\frac{\omega_{\mathrm{opt}}^2}{v_a}\left[\left(\frac{\omega_a}{v_a}\right)^2-\left(\frac{\omega_a}{v_a}\right)^2_{\mathrm{thr}}\right]\equiv\frac{\omega_{\mathrm{opt}}^2}{v_a}\Delta, \tag{15}$$

where $\omega_{\mathrm{opt}}\approx v_a\delta/y_m$.

Let us estimate the characteristics of the unstable waves. Taking $\delta\le1$ and $D_i\approx0.1$ m^2/s we obtain from (12) that $V_{\mathrm{thr}}\approx2$ m/s, and for y_m between 0.1 and 1 the characteristic irregularity scales from (14) are λ_{opt} between 0.3 and 5 m. Then, the radial component of the velocity observed by the radar is up to 40 m/s toward the radar (Figures 3d and 4). For numerical estimation we take the vertical velocity of the dust 10 m/s, which does not contradict to the observations. For such a velocity, with taking into account that $k^2r_{Di}^2<<1$ we obtain from (13) $\sqrt{Z}\sim2.4/\sqrt{P}$, which mean $Z\approx6$ for $P\le1$. This value of Z agrees with the previous estimation from equation (8). Finally, we estimate the instability growth rate using (15) and with $\Delta=0.1$, $\gamma_m\approx10$ Hz. Therefore, the instability may generate meter-scale irregularities with a time scale on the order of 0.1 s, which agrees with the observations.

To estimate applicability of the model, we used typical parameters of winter mesosphere. However, size and density of aerosol particles might vary in very large ranges. Indeed, huge amount of fuel from the 36.8 t rocket was spread over the area of hundreds kilometers. Hence, various densities of aerosols, i.e., values of parameter P in (9), might occur. As far heavier particles sedimented faster, separation of particles on size must occur so that particles of certain size might prevail at some time and place. Obviously, the radar detections could occur from those places and at that time where and when size and density of the aerosols were suitable for generation of irregularities.

5.3. Comparison With PMSE

Originally, the model of *Trakhtengerts* [1994] was suggested to explain electron density irregularities responsible for the polar mesospheric summer echo (PMSE). Such irregularities occur at altitudes on the order of 85–87 km and are associated with aerosol ice particles in the cold (on the order of 100–120 K) summer mesosphere. The size and charge of the ice particles were assumed to be $r_a \approx 200$ nm and $Z \approx 10^3$, respectively.

In the present paper we used the model as a possible mechanism that might explain effects observed in the mesosphere after the missile explosion in the upper thermosphere. There are several differences from the PMSE. First, the mass density of aluminum oxide particulates is 2–3 times larger than that of ice. Second, the irregularities were detected at 80 km altitude, which is lower than PMSE. Third, the event occurred in the warm (about 220 K) mesosphere. Most important parameter for generation of PMSE is temperature. In the condition that the neutral temperature is less than 150 K, ice particles causing PMSE can be generated [e.g., *Rapp and Lübken*, 2004]. For this current event, temperature was quite higher than 150 K, so that ice particles which play major role in generation of PMSE could not exist. However, the aerosol particles of the rocket remains were able to play their role in generation of the electron density irregularities. Fourth, for the particulates of the 100 nm size we obtained that the orbit motion limited theory allows a charge on the order of 5–6 elementary units, which is essentially less than that assumed for PSME. Nevertheless, numerical estimations show that the mechanism may be effective even for such different parameters and conditions.

6. Summary

The Russian military missile Bulava is a solid propellant 36.8 t ballistic rocket. On 9 December 2009 at about 07 UT because of a technical problem such a missile was self-destroyed at a distance of about 500 km to the east of SGO. The ionosonde and meteor radar observations at SGO were presented in *Kozlovsky et al.* [2014], where the focus was on the processes of transport (spreading) of the remains of the missile in the ionosphere, but a detailed investigation of the MR reflections was out the scope of that paper. The present paper is an attempt to investigate a specific reflection of the meteor radar signals from the irregularities caused by the scattered remains of the exploded missile.

The missile was self-destroyed at a height of 170–260 km within a radius of 500 km from SGO. After 2–3 h the SGO meteor radar, operating at a frequency 36.9 MHz, received unusual echoes, which indicate turbulence of ionospheric plasma, or irregularities of electron density with temporal scale on the order of 0.1 s and spatial scale of a few to tens of meters. The turbulence occurred at a height of about 80 km and was localized in areas of about 60 km in a horizontal dimension. Line-of-sight velocity of the irregularities was up to a few tens of meters per second toward the radar. The event occurred in the warm (about 220 K) high-latitude winter mesosphere during extremely low solar and geomagnetic activity. We conclude that aerosol particles caused by the missile explosion played a key role in producing the electron density irregularities.

As a possible explanation, we suggest that sedimented by gravity and, hence, moving with respect to the air, charged aerosol particles (presumably of 100 nm radius and composed of aluminum oxide) might produce meter-scale irregularities (electrostatic waves) via dissipative instability, which mechanism is analogous to that of the resistive beam-plasma instability. This mechanism does not require additional assumptions on the turbulence of neutral atmosphere. The presented numerical estimations based on the model of *Trakhtengerts* [1994] show that this hypothesis is realistic, although we are unable to rule out another unknown mechanism.

Acknowledgments
Data of the meteor radar are available from SGO (http://www.sgo.fi/). S.S. acknowledges support from the Academy of Finland grant 287916. M.L. acknowledges support from Natural Environment Research Council grant NE/K011766/1.

References

Bernhardt, P. A., J. B. Baumgardner, A. N. Bhatt, P. E. Erickson, M. F. Larsen, T. R. Pedersen, and C. L. Siefring (2011), Optical emissions observed during the charged aerosol release experiment (CARE I) in the ionosphere, *IEEE Trans. Plasma Sci.*, *39*, 2774–2775, doi:10.1109/TPS.2011.216494.

Bernhardt, P., et al. (2012), Ground and space-based measurement of rocket engine burns in the ionosphere, *IEEE Trans. Plasma Sci.*, *40*(5), 1267–1286.

Brasseur, G., and S. Solomon (1984), *Aeronomy of the Middle Atmosphere: Chemistry and Physics of the Stratosphere and Mesosphere*, 414 pp., D. Reidel, Dordrecht, Netherlands, doi:10.1007/978-94-009-6401-3.

Chau, J. L., I. Strelnikova, C. Schult, M. M. Oppenheim, M. C. Kelley, G. Stober, and W. Singer (2014), Nonspecular meteor trails from non-field-aligned irregularities: Can they be explained by presence of charged meteor dust?, *Geophys. Res. Lett.*, *41*, 3336–3343, doi:10.1002/2014GL059922.

Chernouss, S. A., Y. V. Platov, V. V. Alpatov, and M. V. Uspensky (2012), Optical phenomena due to rocket exhaust products in the atmosphere, *Geophysica*, *48*(1–2), 65–79.

Fortov, V. E., I. Iakubov, and A. Khrapak (2006) *Physics of Strongly Coupled Plasma*, p. 520, Oxford Univ. Press, Oxford.

Hocking, W. K., B. Fuller, and B. Vandepeer (2001), Real-time determination of meteor-related parameters utilizing modern digital technology, *J. Atmos. Sol. Terr. Phys.*, *63*, 155–169.

Kaifler, N., B. Kaifler, B. Ehard, S. Gisinger, A. Dörnbrack, M. Rapp, R. Kivi, A. Kozlovsky, M. Lester, and B. Liley (2017), Observational indications of downward-propagating gravity waves in middle atmosphere lidar data, *J. Atmos. Sol. Terr. Phys.*, Available online 10 March 2017, doi:10.1016/j.jastp.2017.03.003.

Klumov, B. A., G. E. Morfill, and S. I. Popel (2005), Formation of structures in a dusty ionosphere, *J. Exp. Theor. Phys.*, *100*(1), 152–164, doi:10.1134/1.1866207.

Kozlovsky, A., and M. Lester (2015), On the VHF radar echoes in the region of midnight aurora: Signs of ground echoes modulated by the ionosphere, *J. Geophys. Res. Space Physics*, *120*, 2099–2109, doi:10.1002/2014JA020715.

Kozlovsky, A., S. Shalimov, R. Lukianova, and M. Lester (2014), Ionospheric effects of the missile destruction on 9 December 2009, *J. Geophys. Res. Space Physics*, *119*, 3873–3882, doi:10.1002/2013JA019531.

Lukianova, R., A. Kozlovsky, S. Shalimov, T. Ulich, and M. Lester (2015), Thermal and dynamical perturbations in the winter polar mesosphere-lower thermosphere region associated with sudden stratospheric warmings under conditions of low solar activity, *J. Geophys. Res. Space Physics*, *120*, 5226–5240, doi:10.1002/2015JA021269.

Plane, J. M. C. (2002), Laboratory studies of meteoric metal chemistry, in *Meteors in the Earth's Atmosphere*, edited by E. Murad and I. P. Williams, pp. 289–309, Cambridge Univ. Press, Cambridge.

Platov, Y. V., S. A. Chernouss, and V. V. Alpatov (2013), Features of optical phenomena connected with launches of solid-propellant ballistic rockets, *Geomagn. Aeron.*, *53*, 198–203.

Rapp, M., and F.-J. Lübken (2004), Polar mesosphere summer echoes (PMSE): Review of observations and current understanding, *Atmos. Chem. Phys.*, *4*, 2601–2633.

Robertson, S., S. Dickson, M. Horányi, Z. Sternovsky, M. Friedrich, D. Janches, L. Megner, and B. Williams (2014), Detection of meteoric smoke particles in the mesosphere by a rocket-borne mass spectrometer, *J. Atmos. Sol. Terr. Phys.*, *118*, 161–179, doi:10.1016/j.jastp.2013.07.007.

Shepherd, M. G., W. F. J. Evans, G. Hernandez, D. Offermann, and H. Takahashi (2004), Global variability of mesospheric temperature: Mean temperature field, *J. Geophys. Res.*, *109*, D24117, doi:10.1029/2004JD005054.

Silant'yev, A. I. (1964), *Solid Rocket Propellants*, p. 80, Voenizdat, Moscow, Russia.

Spell, T. (2009), Estimation of the location, trajectory, size, and altitude of the "Norway spiral" phenomenon. [Available at http://www.spellconsulting.com/reality/Norway_Spiral.html.]

Trakhtengerts, V. Y. (1994), Generation mechanism of polar mesosphere summer echoes, *J. Geophys. Res.*, *99*, 21,083–21,088, doi:10.1029/93JD03280.